Stability of Schottky contacts with Ta–Si–N amorphous diffusion barriers and Au overlayers on 6H–SiC

I. Shalish[a)] and Yoram Shapira
Department of Electrical Engineering–Physical Electronics, Tel-Aviv University, Tel-Aviv 69978, Israel

The thermal stability of two sputter-deposited Schottky contact metallizations incorporating Ta–Si–N amorphous diffusion barriers and Au overlayers are compared using depth profiling by backscattering spectrometry and secondary ion mass spectrometry as well as current–voltage measurements. A $\langle$6H–SiC$\rangle$/TaSi$_2$/Ta$_{20}$Si$_{40}$N$_{40}$/Au metallization changes its Schottky barrier height from 0.71 to 0.62 eV upon annealing at 600 °C for 30 min, while its ideality factor improves from an initial value of 1.55 to 1.16. Both Schottky barrier height and ideality factor remain stable upon successive annealing of the sample at 700 °C for 30 min and for an additional 90 min. The observed stability is attributed to the thermal stability of TaSi$_2$ with SiC and to the effectiveness of the Ta–Si–N diffusion barrier evidenced in backscattering depth profiles. On the other hand, a $\langle$6H–SiC$\rangle$/Ta$_{36}$Si$_{14}$N$_{40}$/Au metallization that does not include the silicide contacting layer becomes ohmic after vacuum annealing at 600 °C for 30 min, while no signs of metallurgical interaction are observed in its backscattering spectra. Using secondary ion mass spectrometry, diffusion of nitrogen is observed from the Ta–Si–N layer into the 6H–SiC substrate. It is tentatively suggested that nitrogen penetrates the substrate through defects, induced in the sputter-deposition process. © *2000 American Vacuum Society.* [S0734-211X(00)03005-5]

I. INTRODUCTION

Today's high power and high-temperature semiconductor devices are based mainly on silicon and GaAs. The temperature limit for continuous operation of silicon- and GaAs-based devices is known to be 300 and 460 °C, respectively, when special fabrication measures and precautions are taken in their production.[1,2] For automotive, avionics, space, and high density packaging applications, there is a need for electronic devices that can operate at 600 °C. Wide band gap semiconductors are the natural choice for high-temperature applications, as they provide lower intrinsic carrier concentration at a given temperature and thereby a large temperature range over which a p–n junction can exist.

Among the wide band gap materials that are available over an adequate range of doping and sufficiently low defect density, silicon carbide offers the widest band gap, a high thermal conductivity (4.9 W/cm K), and an avalanche breakdown field (3×10^6 V/cm), which is an order of magnitude larger than that of silicon. Silicon carbide occurs in many polytypes differing from one another only in the stacking sequence of the double close-packed layers of Si and C atoms.[3] The three most common polytypes of silicon carbide are 3C–SiC ($Eg = 2.2$ eV), 4H–SiC ($Eg = 3.2$ eV), and 6H–SiC ($Eg = 2.86$ eV). The interest in the 6H polytype has grown rapidly in the last decade, owing to new growth techniques, which made available epitaxial layers grown on bulk material.[4]

In view of the high chemical stability and low intrinsic carrier concentration of the silicon carbides, their high-temperature applications will be limited by the stability and the reliability of the contact metallization. The thermal stability of several metal/SiC contacts has been studied and in most of them the metals have been found to react with SiC at elevated temperatures. Schottky barrier height measurements have been made mostly on as-deposited samples. In the few reported cases where long thermal treatments (>20 min) at temperatures higher then 500 °C were applied, the Schottky diodes characteristics were found to change due to a metal–semiconductor reaction.[5]

A convenient way to achieve thermodynamically stable metallization is to use inert conductive materials or materials that are known to be chemically stable with the substrate, e.g., silicon-rich silicides. Reactions of SiC with transition metals commonly result in a mixture of phases at the contact. One way to avoid such a poly-phased contact is to sputter deposit the desired silicide using a silicide target. However, a sputter-deposited silicide possesses polycrystalline microstructure, and thus may not be able to prevent diffusion of Au from the interconnect layer and its reaction with the SiC substrate (Au–SiC reaction has been observed already at 300 °C).[6] To that end, various diffusion barrier materials have been tested.[7,8]

Ta–Si–N belongs to a class of ternary amorphous films of the type TM–Si–N (TM=Ta, Ti, Mo, W). These films stand out in their excellent performance as barrier materials, preventing the interdiffusion or reaction between Al, Cu, or Au and Si. Amorphous diffusion barriers are the most promising candidates for high-temperature metallizations as they do not possess extended defects of the kind that provide fast diffusion paths in polycrystalline materials.[9]

In this article, we examine and compare the thermal stability of two complete metallization schemes incorporating a Ta–Si–N layer as a diffusion barrier between a Au overlayer and a 6H–SiC substrate both with and without a contacting

[a)]Current address: Division of Engineering and Applied Sciences, Harvard University, Cambridge, MA 02138; electronic mail: shalish@deas.harvard.edu

TaSi$_2$ layer. The purpose of this study is twofold: (1) to confirm the applicability of Ta–Si–N as barrier layers between Au and TaSi$_2$ or 6H–SiC, and (2) to determine whether the thermal stability of the $\langle$6H–SiC$\rangle\backslash$TaSi$_2$ and $\langle$6H–SiC$\rangle\backslash$Ta–Si–N contacts also applies to their electrical characteristics.

II. EXPERIMENTAL DETAILS

The 6H–SiC wafer, used in this work, was purchased from CREE Research, Inc. The wafer was n-type, 280 μm thick, with a 10-μm-thick n-type epilayer grown on its silicon face. The substrate and the epilayer were nitrogen doped with doping levels of 7.3×10^{17} and 1×10^{16} cm^{-3}, respectively. Prior to deposition, the samples were degreased in organic solvents in an ultrasonic bath (trichlorethylene, acetone, and methanol, sequentially). Circular diodes of three different diameters (0.05, 0.1, and 0.25 cm) were fabricated by photolithographic patterning and lift-off. The samples were etched in a 10% HF solution for 10 s to clean up the contact windows and dried in N$_2$ gas just prior to deposition. All films in this study were deposited by rf sputtering using a planar magnetron cathode of 7.5 cm in diameter. The substrate plate was placed 7 cm below the target and was neither cooled nor heated externally. The sputtering system is equipped with a cryopump and a cryogenic baffle with a base pressure of 4×10^{-7} Torr.

The TaSi$_2$ layers were deposited in Ar at 10 mTorr total pressure and 300 W root-mean-square (rms) forward sputtering power. The Ta–Si–N films were deposited in a discharge of Ar/N$_2$ gas mixture at a N$_2$ to Ar flow ratio of 0.036 and a total gas pressure of 10 mTorr. The Au overlayers films were deposited at 5 mTorr total pressure and 200 W rms from elemental targets. The flow of Ar and the total gas pressure were adjusted by mass flow controllers and monitored with a capacitive manometer in a feedback loop.

Annealing was done after the deposition in an evacuated tube furnace (at 5×10^{-7} Torr). Samples for backscattering and for secondary ion mass spectrometry (SIMS) were processed concurrently with the diode samples.

To eliminate a possible effect of the top layers on the Schottky barrier characteristics, reference diode samples, incorporating the contact metallization alone, were prepared and heat-treated concurrently with the complete metallization samples.

Before and after the thermal annealing, the diode samples were characterized by current–voltage (I–V) measurements to determine the Schottky barrier height and the ideality factor. The I–V characteristics were measured using a HP-4145A parameter analyzer and were performed at room temperature. An indium–gallium alloy was used as a back contact. In all samples, it was verified that the current scaled with the area of the diode. This proves that it is the metal/epilayer interface that determines the I–V characteristics (and not the back contact), and that the current is not due to a peripheral leakage but flows across the area of the contact. The I–V characteristics were analyzed using the thermionic emission model. Lien's method[10] was employed to calculate

the series resistance, followed by a least-squares fit of the corrected I vs V–IR curve to obtain the saturation current density (J_s) and the ideality factor. The barrier height was calculated from the equation[11]

$$\Phi_B = \frac{kT}{q}\ln\left(\frac{A^{**}T^2}{J_s}\right),\tag{1}$$

where $A^{**}=72$ A/cm^2 K^2 is the effective Richardson constant for 6H–SiC.

The backscattering samples were characterized by 2 MeV ^{4}He^{++} backscattering spectrometry to determine compositional profiles and monitor interdiffusion or reactions in the samples. The thickness of the Au layers was estimated from the elemental bulk density and energy losses in the backscattering spectra. The thickness of TaSi$_2$ and Ta–Si–N layers was estimated from the sputtering rates previously calibrated using profilometry of thick samples. The compositions of the Ta–Si–N layers were calculated from the relative signal heights of the elements in backscattering spectra of thicker films, deposited under the same sputtering conditions on graphite substrates. These, however, are but rough estimates, with a typical error of $\sim20\%$. Due to the small size of the samples, variations in the ^{4}He^{++} ion beam direction, and insufficient beam focusing, a spurious signal from the carbon sample holder in addition to that of the samples could not be avoided. Hence, the conventional total charge method to calibrate the spectral yield could not be applied. Therefore, the spectra were calibrated by integrating counts from the surface energy of carbon (0.505 MeV) up to 2.0 MeV, assuming that mass was conserved.

Secondary ion mass spectroscopy (SIMS) was carried out in a CAMECA IMS4f ion microscope. An Cs$^+$ primary ion beam with an impact energy of 14.5 keV was used to monitor the ^{12}C$^+$, ^{14}N$^+$, ^{16}O$^+$, ^{30}S$^+$, and ^{181}Ta$^+$ secondary ions. The diameter of the analyzed area was 60 μm, while the primary beam was rastered over an area of 250×250 μm^2. The measurement was repeated in four different spots on each sample to assess the lateral uniformity. The top Au layer was selectively etched from the samples before the introduction into the measurement chamber. The depth was estimated with ±10 nm accuracy from the depth of the SIMS crater using α-step profilometer.

III. RESULTS

A. $\langle$6H–SiC$\rangle$/TaSi$_2$(50 nm)/Ta$_{20}$Si$_{20}$N$_{40}$(80 nm)/Au(50 nm)

Figure 1 shows the backscattering depth profiles obtained from a $\langle$6H–SiC$\rangle$TaSi$_2$(50 nm)/Ta$_0$Si$_{20}$N$_{40}$(80 nm)/Au(50 nm) sample, before and after 30 min annealing in vacuum at 700 °C. Except for changes below the carbon surface energy, the spectra overlap within the experimental error. The surface carbon signal is a spurious signal resulting from an unfocused beam impinging on the carbon sample holder. Conversely, the forward I–V characteristics of $\langle$6H–SiC$\rangle$/TaSi$_2$(50 nm)/Ta$_{20}$Si$_{20}$N$_{40}$(80 nm)/Au(50 nm) Schottky diodes do change after 30 min annealing in vacuum
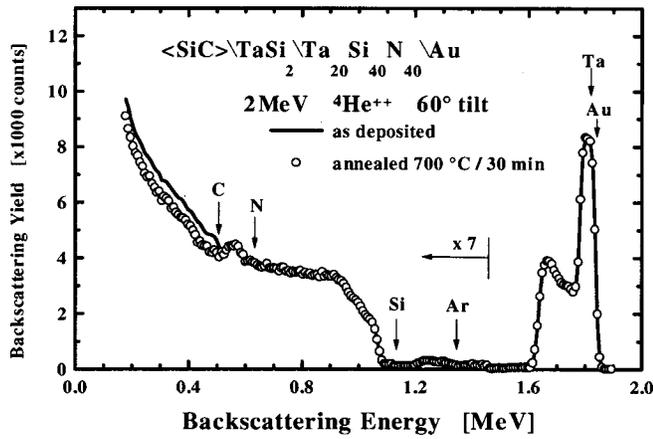
FIG. 1. 2 MeV ^{4}He^{++} backscattering spectra of $\langle$6H–SiC$\rangle$/TiSi$_2$/Ta$_{20}$Si$_{40}$N$_{40}$/Au before and after annealing in vacuum at 600 °C for 30 min.

FIG. 3. 2 MeV ^{4}He^{++} backscattering spectra of $\langle$6H–SiC$\rangle$/Ta$_{36}$Si$_{14}$N$_{50}$/Au before and after annealing in vacuum at 600 °C for 30 min.

at 600 °C from a barrier height of 0.70 to 0.61 eV and from an ideality factor of 1.55 to 1.16. However, no significant changes were observed upon further annealing for an additional 90 min at 700 °C (Fig. 2). To eliminate possible role of the two top layers, $I-V$ measurements were made also on $\langle$6H–SiC$\rangle$/TaSi$_2$(100 nm) before and after the same heat treatment. The results were the same as for the complete metallization within the experimental error.

B. $\langle$6H—SiC$\rangle$/Ta$_{36}$Si$_{14}$N$_{50}$(80 nm)/Au(45 nm)

As we discuss later, SiC and Ta–Si–N barrier material may be expected to provide an inert contact up to at least 700 °C. Therefore, it seems reasonable to expect that omission of the TaSi$_2$ layer should not affect the thermal stability of the metallization, while providing a less complex structure. To test this hypothesis, $\langle$6H–SiC$\rangle$/Ta$_{36}$Si$_{14}$N$_{50}$(80 nm)/Au(45 nm) samples were deposited and annealed for 30 min in vacuum at 600 °C. Figure 3 shows the backscattering spectra before and after the annealing. Indeed, as expected, no change is observed upon annealing and the spectra over-
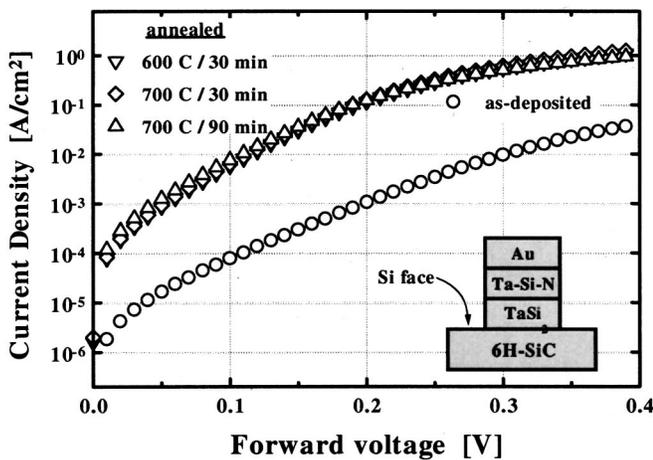
lap, within the experimental accuracy. However, $I-V$ characteristics change considerably after the same annealing. Figure 4 compares two $I-V$ curves of a typical $\langle$6H–SiC$\rangle$/Ta$_{36}$Si$_{14}$N$_{50}$(80 nm)/Au(45 nm) diode before and after annealing. As deposited, the diodes possess a Schottky barrier of 0.76 eV and an ideality factor of 1.27. After annealing the $I-V$ characteristics become ''soft'' with a high leakage current. The same ''softening'' was observed after annealing in $\langle$6H–SiC$\rangle$/Ta$_{36}$Si$_{14}$N$_{50}$/80 nm) diodes as well, eliminating a possible role of the Au overlayer.

The most prominent difference between the Ta–Si–N/SiC system and the TaSi$_2$/SiC system is the addition of nitrogen. Since backscattering has a low sensitivity to light elements, we complemented it with SIMS. Two $\langle$6H–SiC$\rangle$/Ta$_{36}$Si$_{14}$N$_{50}$(80 nm)/Au(45 nm) samples were used for SIMS. One was kept as reference, while the other was annealed in vacuum for 2 h at 600 °C. The top Au layer was then etched and the samples were introduced into the SIMS vacuum chamber. SIMS depth profiles were obtained from four different points on each sample. The only element for which a

FIG. 2. A semilogarithmic $I-V$ plot of $\langle$6H–SiC$\rangle$/TiSi$_2$/Ta$_{20}$Si$_{40}$N$_{40}$/Au diode forward characteristics as deposited and after successive vacuum anneals at 600 and 700 °C.
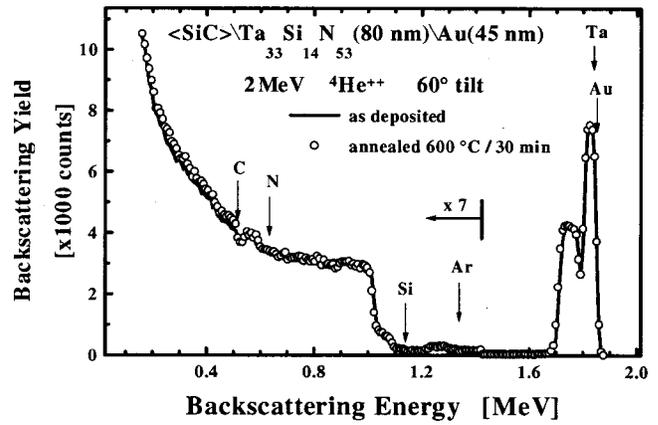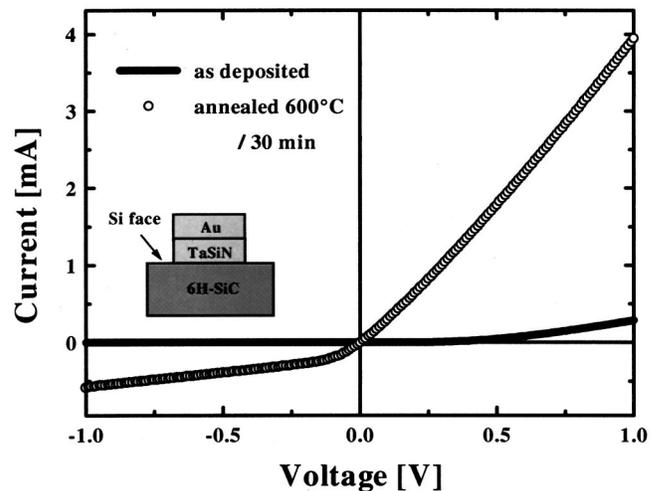

FIG. 4. $I-V$ characteristics of $\langle$6H–SiC$\rangle$/Ta$_{36}$Si$_{14}$N$_{50}$/Au before and after annealing in vacuum at 600 °C for 30 min.
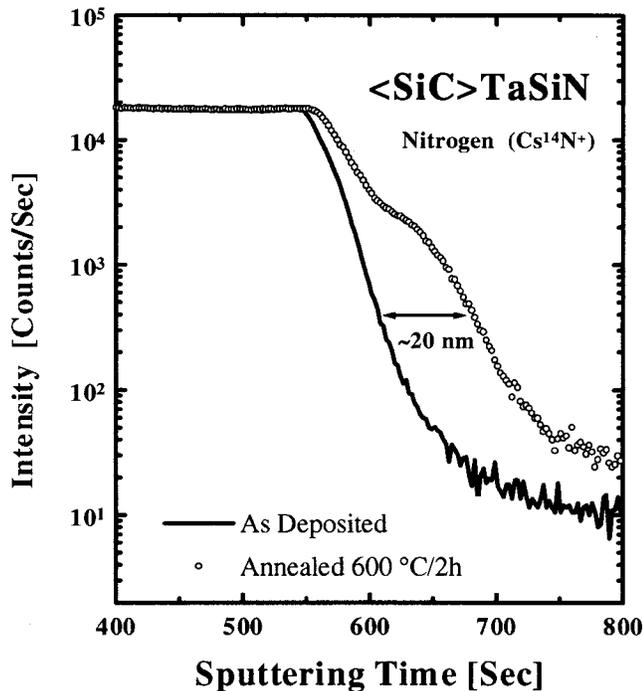
FIG. 5. Secondary ion mass spectroscopy depth profiles of nitrogen in $\langle$6H–SiC$\rangle$/Ta$_{36}$Si$_{14}$N$_{50}$ obtained from an as-deposited sample and from a sample annealed for 2 h in vacuum at 600 °C. The data presented depicts the most significant nitrogen diffusion observed. Other spots on the same annealed sample showed less diffusion or no diffusion at all.

difference was observed between the as-deposited and annealed depth profiles was nitrogen. However, the diffusion was not laterally uniform. Figure 5 compares the nitrogen SIMS depth profiles from an as-deposited sample and from annealed sample. The diffusion profile was obtained by subtracting the depth profile of nitrogen in the as-deposited sample from that of the annealed sample to eliminate the typical smearing of the depth profile. The resulting diffusion profile is shown in Fig. 6, where $x=0$ represents the metal–
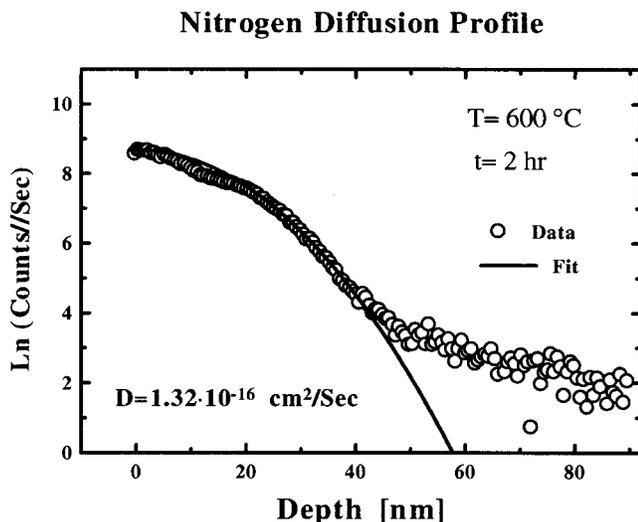

FIG. 6. Nitrogen diffusion profile obtained from Fig. 5 by subtraction of the as-deposited profile from that of the annealed sample. $x=0$ is the metal–semiconductor interface.

semiconductor interface. Assuming limited-source diffusion, the concentration can be described by the equation[12]

$$N(x,t) = N_0 \exp\left(-\frac{x^2}{4Dt}\right), \qquad (2)$$

where x is the depth, t is the annealing time ($t=7200$ s), and D is the diffusion coefficient. Using Eq. (2) the nitrogen diffusion profile was found to fit a diffusion coefficient of $D=1.32\times10^{-16}$ cm^2/s.

IV. DISCUSSION

The stability of TaSi$_2$ in contact with SiC is known *a priori* from the phase diagram. The 1000 °C isothermal section of the Ta–Si–C phase diagram experimentally determined by Schuster[13] shows a tie-line between the TaSi$_2$ phase and SiC. The backscattering depth profiles in Fig. 1 confirm this stability for the specific case of sputter-deposited TaSi$_2$ and 6H–SiC. However, in our case the TaSi$_2$ phase is a layer deposited onto the substrate, so that the quality of the interface is dependent on the substrate cleaning and preparation. It is likely that contamination, which may be too thin to be detected by backscattering, is present at the interface, and is responsible for the ideality factor of 1.55 in the as-deposited diodes. Another possible cause for the observed ideality factor may be Ar trapped in the contacting layer during the sputter-deposition process. Trapped Ar is typical of sputter-deposited films and is also evidenced in our backscattering spectra. Small atomic rearrangement at the interface, e.g., redistribution of the trapped Ar or interface impurities, could account for the improvement of the ideality factor from 1.55 to 1.16 after the initial annealing at 600 °C. Obtaining the same results for a $\langle$6H–SiC$\rangle\backslash$TaSi$_2$ both with and without the Ta–Si–N layer and the top Au ensures that these layers do not contribute to the process responsible for the initial changes. In any case, these changes are limited to the initial annealing, following which both the Schottky barrier height and the ideality factor remain stable after additional 90 min of annealing at 700 °C. This adds to the depth profiling results in showing that the TaSi$_2\backslash$Ta–Si–N$\backslash$Au indeed provides the desired thermal stability.

However, the preparation of a TaSi$_2\backslash$Ta–Si–N$\backslash$Au metallization requires a sequential deposition of three different materials. As both SiC and Ta–Si–N are refractory materials, one may wonder whether the contacting TaSi$_2$ layer is a necessary added complexity. Indeed, the backscattering spectra of Fig. 3 seem to confirm the expected stability of 6H–SiC with Ta–Si–N at 600 °C. This apparent metallurgical stability, however, turns out to be insufficient to support the stability of the Schottky barrier, which is found to soften after the same heat treatment.

Since major compositional changes at the interface are ruled out by backscattering, the remaining possible mechanism that could account for the observed Schottky barrier lowering is doping. Defect formation cannot be expected to contribute to the doping, as defects are usually removed by the annealing (i.e., annealed-out).[14] It is therefore diffusion

that remains to be considered. Out of the three available elements in the neighboring Ta–Si–N layer, nitrogen seems the most probable diffusant for three reasons. First, it is the smallest and most mobile element in the system; second, nitrogen is the natural dopant of SiC: it is present even in undoped SiC;[15] and third, nitrogen is the only element out of the three that is missing in the stable $TaSi_2$ contact. Thus, it is not surprising that nitrogen was the only species found by SIMS to redistribute after the annealing (Fig. 5). However, conventional application of diffusion-based doping techniques in SiC was shown to require high temperatures (over 1800 °C).[16] Diffusion coefficients of nitrogen in SiC were found to range from 2×10^{-16} cm^2/s at 2000 °C to 5×10^{-12} cm^2/s at 2600 °C.[17] This renders the possibility of nitrogen diffusion into bulk 6H–SiC highly unlikely at a temperature of 600 °C. For diffusion to take place at this temperature defects have to be present. Diffusion through defects may require a much lower activation energy then bulk diffusion.[18] Lossy *et al.* show that implantation damage enhances nitrogen implant diffusion in 3C–SiC.[19] They estimated an activation energy of 0.91 eV and a pre-exponential factor of 3.1×10^{-11} cm^2/s. Using their data, a diffusion coefficient of 2.65×10^{-16} cm^2/s is obtained for annealing at 600 °C, which is of the order of the value observed in this work (1.32×10^{-16} cm^2/s).

One possible mechanism for defect formation is the sputter-deposition process. Sputter deposition has been found to introduce defects in Si.[20,21] These defects are formed in the proximity of the interface,[22] and may therefore account for the shallowness of the observed nitrogen diffusion into the SiC substrate. This process may be even further limited by the annealing out of the sputter-induced defects taking place concurrently with the diffusion. Itoh *et al.* have shown that irradiation damage in SiC is completely annealed out when heat-treated in the temperature range between 600 and 800 °C.[23] We therefore suggest that nitrogen, originating at the Ta–Si–N layer, diffuses into the substrate via sputter-induced defects. Thus, it may be responsible for the observed softening of the Schottky barrier by increasing the doping at the interface.

Sputter-damage-assisted doping from contacting layers of nitrides, such as Ta–Si–N, may prove useful in producing ohmic contacts to *n*-type SiC, circumventing the need for implantation, if this process can be tuned to yield the required contact resistivities. This, however, remains a subject for further investigation.

V. CONCLUSION

Depth profiling and forward $I-V$ measurements were used to study the thermal stability of two rf-sputtered metallizations for 6H–SiC. In both cases, Ta–Si–N layers proved to be an effective barrier to Au diffusion. $TaSi_2$ is thermally stable in contact with SiC and demonstrates stable $I-V$ characteristics for at least 2 h of annealing at 700 °C. However, the thermal stability of the contacting layer by itself is insufficient to prevent changes in the Schottky barrier upon initial annealing. Minor thermally induced interfacial atomic rear-

rangements, too small to be detected by backscattering can evidently alter the electronic transport across the SiC/metal interface significantly. In the case of the $TaSi_2$ contacting layer, this change results in a more ideal Schottky barrier, that remains stable thereafter. However, when the $TaSi_2$ is omitted in favor of a direct contact of the Ta–Si–N and the SiC substrate, the rectifying character of the contact is severely compromised upon annealing at 600 °C. Based on SIMS depth profiles, this change is attributed to a shallow penetration of nitrogen, originating from the Ta–Si–N, into the substrate, probably via sputter-induced defects. This nitrogen diffusion increases the doping and thus narrows the Schottky barrier.

[1] F. S. Schucair and P. K. Ojala, IEEE Trans. Electron Devices **39**, 1551 (1992).
[2] J. L. Prince, B. L. Draper, E. A. Rapp, J. N. Kronberg, and L. T. Fitch, IEEE & CHMT **CHMT-3**, 571 (1980).
[3] R. Verma and P. Krishna, in *Plymorphism and Polytypism in Crystals* (Wiley, New York, 1966).
[4] H. Morkoc, S. Strite, G. B. Gao, M. E. Lin, B. Sverlov, and M. Burns, J. Appl. Phys. **76**, 1363 (1994).
[5] For review, see: L. M. Porter and R. F. Davis, Mater. Sci. Eng., B **34**, 83 (1995).
[6] D. E. Ioannou, N. A. Papanicolaou, and P. E. Nordquist, Jr., IEEE Trans. Electron Devices **ED-34**, 1694 (1987).
[7] E. D. Luckowski, J. M. Delucca, J. R. Williams, S. E. Mohney, M. J. Bozack, T. Isaacs-Smith, and J. Crofton, J. Electron. Mater. **27**, 330 (1998).
[8] R. Wenzel, F. Goesmann, and R. Schmid-Fetzer, J. Mater. Sci.: Mater. Electron. **9**, 109 (1998).
[9] M.-A. Nicolet, Appl. Surf. Sci. **91**, 269 (1995).
[10] C. D. Lien, F. C. T. So, and M.-A. Nicolet, IEEE Trans. Electron Devices **ED-31**, 1502 (1984).
[11] F. A. Padovani and R. Stratton, Solid-State Electron. **9**, 695 (1966).
[12] R. C. Jaeger, *Introduction to Microelectronic Fabrication* (Addison-Wesley, New York, 1988), p. 49.
[13] J. C. Schuster, J. Chem. Phys. **90**, 373 (1993).
[14] J. Schneider and K. Maier, Physica B **185**, 199 (1993).
[15] J. B. Casady and R. W. Johnson, Solid-State Electron. **39**, 1409 (1996).
[16] Y. A. Vodakov and E. N. Mokhov, in *Silicon Carbide*, edited by R. C. Marshall, J. W. Faust, Jr., and C. E. Ryan (University of South Carolina Press, Columbia, SC, 1973), p. 508.
[17] L. J. Kroko and A. G. Milnes, Solid-State Electron. **9**, 1125 (1966).
[18] L. A. Girifalco, *Atomic Migration in Crystals* (Blaisdell, New York, 1964), p. 32.
[19] R. Lossy, W. Reichert, E. Obermeier, and W. Skorupa, J. Electron. Mater. **26**, 123 (1997).
[20] M. Finetti, I. Suni, M. Bartur, T. Banwell, and M.-A. Nicolet, Solid-State Electron. **27**, 617 (1984).
[21] L. E. Halperin, M. Bartur, E. Kolawa, and M.-A. Nicolet, IEEE Electron Device Lett. **12**, 309 (1991).
[22] H. Wiedersich, in *Surface Modification and Alloying by Laser, Ion, and Electron Beams*, edited by J. M. Poate, G. Foti, and D. C. Jacobson (Plenum, New York, 1983), p. 261.
[23] H. Itoh, N. Hayakawa, I. Nashiyama, and E. Sakuma, J. Appl. Phys. **66**, 4529 (1989).